ChemPubSoc Europe

DOI: 10.1002/cphc.201700967

CHEMPHYSCHEM Communications

Special Issue

Unravelling the Redox-catalytic Behavior of Ce^{4+} Metal–Organic Frameworks by X-ray Absorption Spectroscopy

Simon Smolders,[a] Kirill A. Lomachenko,[b, c] Bart Bueken,[a] Arnaud Struyf,[a] Aram L. Bugaev,[c, d] Cesare Atzori,[d] Norbert Stock,[e] Carlo Lamberti,[c, d] Maarten B. J. Roeffaers,[a] and Dirk E. De Vos*[a]

The introduction of Ce^{4+} as a structural cation has been shown to be a promising route to redox active metal–organic frameworks (MOFs). However, the mechanism by which these MOFs act as redox catalysts remains unclear. Herein, we present a detailed study of the active site in $[Ce_6O_4(OH)_4]$-based MOFs such as Ce-UiO-66, involved in the aerobic oxidation of benzyl alcohol, chosen as a model redox reaction. X-ray absorption spectroscopy (XAS) data confirm the reduction of up to one Ce^{4+} ion per Ce_6 cluster with a corresponding outwards radial shift due to the larger radius of the Ce^{3+} cation, while not compromising the structural integrity of the framework, as evidenced by powder X-ray diffraction. This unambiguously demonstrates the involvement of the metal node in the catalytic cycle and explains the need for 2,2,6,6-tetramethyl-1-piperidinyloxy (TEMPO) as a redox mediator to bridge the gap between the one-electron oxidation of the Ce^{4+}/Ce^{3+} couple and the two-electron alcohol oxidation. Finally, an improved catalytic system with Ce-MOF-808 and TEMPO was developed which outperformed all other tested Ce^{4+}-MOFs.

Metal–organic frameworks (MOFs) are a class of porous crystalline materials constructed from inorganic nodes and organic linkers. Their modularity, high concentration of metal nodes, well-defined porosity and exceptional surface area make MOFs particularly interesting for catalysis, gas sorption and separation.[1–3] One of the most studied MOFs is UiO-66 ($[M_6O_4(OH)_4(bdc)_6]$; bdc = terephthalate; M = Zr^{4+}, Hf^{4+}, Ce^{4+}), a thermally and chemically robust material built up from hexanuclear metal clusters which are 12-fold connected via terephthalate linkers.[4–7] The catalytic performance of UiO-66, attributed to the Lewis acidic metal nodes, has been investigated numerous times.[8–12] Among these, Ce-UiO-66 was reported to act as catalyst for the aerobic oxidation of benzyl alcohol.[13]

Cerium is the cheapest and most abundant rare earth element and has been widely investigated for catalytic applications due to its remarkable redox behavior. It is the only lanthanide with a stable +IV oxidation state due to its vacant f-shell. Ce^{4+} is therefore a strong one-electron oxidant and cerium ammonium nitrate has found many applications as stoichiometric oxidant or homogeneous catalyst.[14,15] CeO_2-containing heterogeneous catalysts are widely applied for the decomposition of NO_x and the oxidation of CO due to the excellent oxygen mobility and oxygen storage capacity of this oxide.[16–18] Hence, CeO_2 particles are often designed as well-defined nano-objects with a focus on maximizing the reactive surface.[19,20] Recently, Lammert et al. reported the synthesis of cerium analogues of several Zr-based MOFs, including UiO-66, containing carboxylate-capped $[Ce_6O_4(OH)_4]^{12+}$ clusters.[13,21–24] With respect to bulk CeO_2, the hexanuclear node in the Ce-UiO-66 framework could be considered as the smallest possible CeO_2 unit, with every Ce cation exposed to the micropores of the material.[25] This expands the catalytic scope of the UiO-66 topology beyond the well-known acid-base activity to include redox reactions, as exemplified by the activity of Ce-UiO-66 in the aerobic oxidation of benzyl alcohol to benzaldehyde.[13] Higher reaction rates were achieved with Ce-UiO-66 than with an equimolar amount of 15 nm CeO_2 nanoparticles. A redox mediator, TEMPO (2,2,6,6-tetramethyl-1-piperidinyloxy) was employed to couple the one-electron reduction of Ce^{4+} to Ce^{3+} with the two-electron alcohol oxidation.[13,26]

The interest in Ce MOFs is mainly driven by their potential redox applicability; unraveling their redox behavior is therefore of great interest. Herein, we study the oxidation state of Ce and the geometry of the hexanuclear cluster in Ce^{4+}-MOFs before and after reaction with TEMPO and benzyl alcohol, since no experimental evidence for the redox change in Ce-MOFs has been provided to date. For this, Ce-UiO-67 was chosen as catalyst, with 4,4′-biphenyldicarboxylate linkers lining the pores. The resulting large pores ensure that reaction

[a] S. Smolders, Dr. B. Bueken, A. Struyf, Prof. M. B. J. Roeffaers, Prof. D. E. De Vos
Centre for Surface Chemistry and Catalysis
Department of Microbial and Molecular Systems (M2S)
KU Leuven, Celestijnenlaan 200F P.O. box 2461
3001 Leuven (Belgium)
E-mail: dirk.devos@kuleuven.be

[b] Dr. K. A. Lomachenko
European Synchrotron Radiation Facility
71 avenue des Martyrs, CS 40220
38043 Grenoble Cedex 9 (France)

[c] Dr. K. A. Lomachenko, A. L. Bugaev, Prof. C. Lamberti
The Smart Materials Research Centre
Southern Federal University, Sladkova 174/28
344090 Rostov-on-Don (Russia)

[d] A. L. Bugaev, C. Atzori, Prof. C. Lamberti
Department of Chemistry, NIS and INSTM Reference Center
University of Turin, Via P. Giuria 7, 10125 Turin (Italy)

[e] Prof. N. Stock
Institut für Anorganische Chemie, Christian-Albrechts-Universität, Max-Eyth Straße 2, 24118 Kiel (Germany)

Supporting Information and the ORCID identification number(s) for the author(s) of this article can be found under https://doi.org/10.1002/cphc.201700967.

An invited contribution to a Special Issue on Reactions in Confined Spaces

can take place in the crystal bulk and not only on the outer surface of the MOF-particles, thereby greatly increasing the number of active sites. The microenvironment around the catalytically active Ce cluster in Ce-UiO-67 is also identical to the one in the previously studied Ce-UiO-66. Ce-UiO-67 was subjected to a solution of 7.5 equiv. TEMPO and 50 equiv. benzyl alcohol in acetonitrile under inert atmosphere to reduce Ce to its +III oxidation state, while avoiding rapid reoxidation to Ce^{4+}.

X-ray absorption near edge structure (XANES) at the Ce L_3- and Ce K-edge was performed to assess the average oxidation state of Ce throughout the whole structure (Figure 1). This type of analysis is very reliable, since XANES features of both Ce L_3- and Ce K-edges are known to be mostly dependent on the average oxidation state of Ce atoms, being much less affected by the variations of local geometry. At the Ce L_3-edge the shape of the spectrum changes dramatically upon transition from Ce^{3+} to Ce^{4+}: while a very sharp single peak is characteristic for the former, the white line of the latter consists of two well-separated maxima of much lower intensity. Spectral features at the Ce K-edge are significantly broader but Ce^{3+} and Ce^{4+} can still be easily distinguished because the edge energy for Ce^{3+} is around 5 eV lower than for Ce^{4+}. The relative concentration of Ce^{3+} in Ce-UiO-67 exposed to the TEMPO/benzyl alcohol mixture (Ce-UiO-67-red) was determined by making a linear combination of a Ce^{3+}-reference, $Ce(NO_3)_3{\cdot}6H_2O$, and a Ce^{4+}-MOF reference, Ce-UiO-66.[13] No measurable Ce^{3+} was present before reaction (Figure S1) but after reduction by the TEMPO/benzyl alcohol mixture, the fraction of reduced Ce was calculated to be 19.4±0.2% and 16.9±0.2% at the Ce L_3 and the Ce K-edge, respectively (Figure 1, Table S1; the reported errors are of statistical origin; the intrinsic error associated to such XANES analyses is in the order of 5%).[27] The best-fit curves are able to remarkably reproduce the experimental data, which is confirmed by the low R-factors (0.0013 at Ce L_3 and 0.0001 at Ce K-edge). The calculated Ce^{3+}-fraction corresponds to an average of approximately one Ce^{3+} ion per hexanuclear cluster (16.7%). This clearly demonstrates that Ce^{4+}-MOFs can accommodate valence changes in the hexanuclear cluster, and hence catalyze redox reactions through the reduction of Ce^{4+} cations. The presence of on average one Ce^{3+} per cluster suggests a structural change that inhibits the reduction of a second cation. Investigating this modification cannot be done from powder X-ray diffraction (PXRD) data because such changes in the cluster are too subtle to accurately determine for porous materials filled with disordered solvent molecules.[5] PXRD however confirmed the conservation of the long-range order in Ce-UiO-67-red (Figure S4).

The exact nature of the active site was therefore studied via extended X-ray absorption fine structure (EXAFS) of Ce-UiO-67-red and compared to the reference Ce-UiO-66, measured at the Ce K-edge (Figure 2a). The amplitude of the EXAFS oscillations was significantly damped compared to the reference, which resulted in lower intensity of the Ce-Ce peak in the Fourier transform (FT) (Figure 2b). To model the observed changes, a fit was carried out in the 3.0–3.9 Å region because the lower-R region had to be excluded due to the very strong contribution of the atomic X-ray absorption fine structure signal which interfered with the Ce-O first shell peaks.[28,29] As a result, the FT shape at low R values is extremely sensitive to background subtraction parameters, which makes precise quantitative analysis very difficult. Conversely, the intensity and position of the Ce-Ce peak were virtually unaffected upon variation of the background spline, which made it a much more reliable indicator.

The EXAFS fit of the reference Ce-UiO-66 compound resulted in a perfect agreement with the geometry of unperturbed cluster with a Ce-Ce coordination number $N_{Ce}=4$ (R-factor of 0.0063). The Ce-Ce distances agreed with the previously reported Ce-UiO-66 structure within 0.01 Å and meaningful values were obtained for both the Debye-Waller (DW) parameter ($\sigma^2_{Ce1}=0.006$ Å^2) and amplitude reduction factor ($S_0{}^2=0.98$).[13] The Ce-Ce peak of Ce-UiO-67-red was however significantly dampened so several models were tested to investigate the origin of the intensity decrease.

First, a fit with fixed N_{Ce} and $S_0{}^2$, obtained from Ce-UiO-66, was performed to test whether the reduced intensity is due to

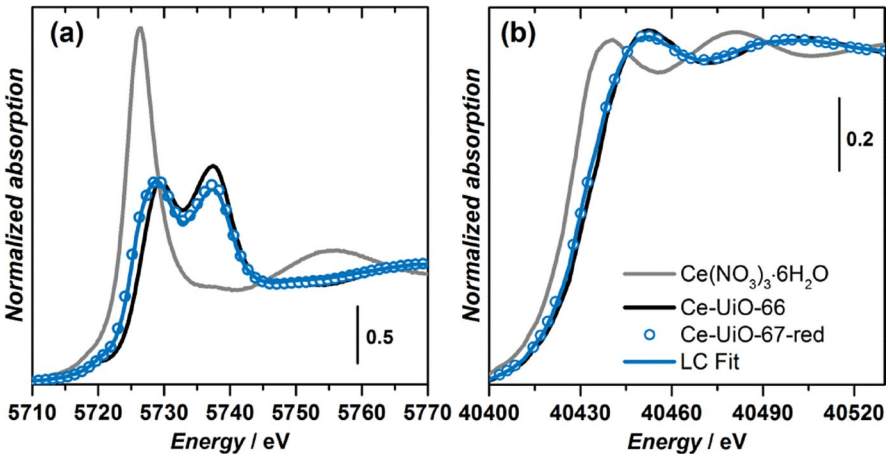

Figure 1. Experimental Ce L_3-edge (a) and Ce K-edge (b) XANES spectra of Ce-UiO-67-red; results of linear combination fitting performed using the spectra of Ce-UiO-66 and Ce^{3+} nitrate as standards.

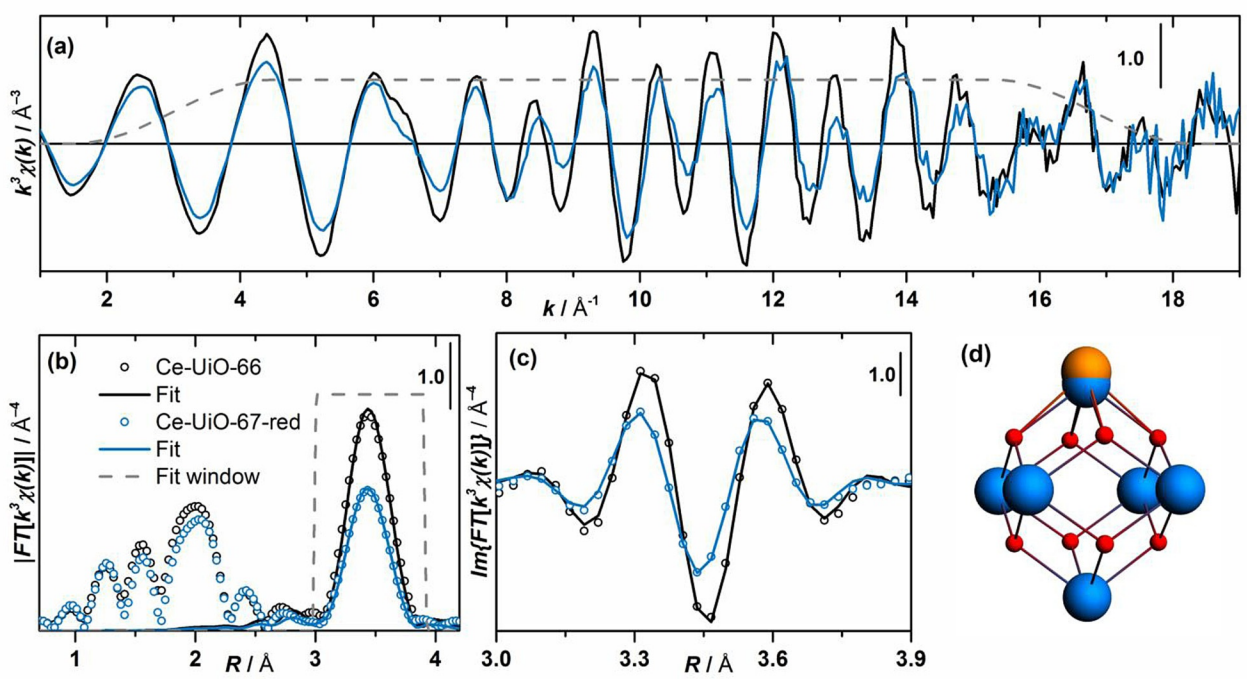

Figure 2. k^3-weighted phase-uncorrected Ce K-edge EXAFS with the Fourier-transform window function (a) and its moduli (b) and imaginary parts (c) for Ce-UiO-66 and Ce-UiO-67-red together with their corresponding fits. For Ce-UiO-67-red the results of the Fit 4 are shown. The range in the panel (c) corresponds to the fitting window (3.0–3.9 Å) shown in the panel (b). Panel (d) schematically illustrates the distortion of the Ce-UiO-67-red cornerstone suggested by Fit 3 (color code: O—red, Ce—blue, perturbed Ce—orange).

an increased uniform (static or dynamic) disorder, which would be reflected by a higher DW value. As expected, the fit resulted in a higher DW factor ($\sigma^2_{Ce1} = 0.0075$ Å^2), but the corresponding large R-factor (0.0310) indicated that the observed damping cannot be explained by a uniform increase of disorder (Fit 1 in Table 1). To simulate anisotropic disorder, expected due to the presence of a Ce^{3+} inside the Ce_6-octahedron, one Ce atom was translated along the octahedron diagonal (Figure 2d). This implies that the 12 Ce-Ce edges of the octahedron are no longer equivalent, but split into 4 long ones and 8 short ones. This model is parametrized in the EXAFS fit by introducing two different Ce-Ce distances with coordination numbers fixed to $N_{Ce1} = 2.67$ and $N_{Ce2} = 1.33$. Both DW factors $\sigma^2_{Ce1} = \sigma^2_{Ce2}$ were fixed to the value obtained from Ce-UiO-66. As expected, the fit resulted in two significantly different Ce-Ce distances, causing the decrease of the EXAFS peak. The R-factor (0.0301) remained however virtually unchanged, which indicated that the quality of the fit was not improved (Fit 2 in Table 1). Repeating this fit with free DW parameters resulted in a strongly decreased R-factor (0.0041) indicating a nearly perfect mathematical fit (Fit 3 in Table 1). However, careful examination of the obtained parameters reveals that, while a short Ce-Ce path was not significantly perturbed, the second path was elongated by 0.3 Å and its DW factor increased to $\sigma^2_{Ce2} = 0.014$ Å^2, which led to an important decrease of the longer path contribution to the examined spectral region. Such numbers are a clear indication that the fitted peak mainly originates from a single Ce-Ce path with a distance close to the reference and a degeneracy significantly lower than 4. Consequently, in Fit 4, only one Ce-Ce path was considered, but the corresponding coordination number, Ce-Ce distance and DW factor were fitted simultaneously. This resulted in a low R-factor (0.0075), close to the one for the unperturbed Ce-UiO-66, and R_{Ce1} and σ^2_{Ce1} values that closely match the reference ones. The obtained coordination number ($N_{Ce} = 2.58$) is very close to the theoretical value of 2.67, which corresponds to the situation where upon interaction with TEMPO

Table 1. Fitting parameters for the Ce K-edge EXAFS spectra of Ce-UiO-66 and Ce-UiO-67-red.

	Ce-UiO-66	Ce-UiO-67-red			
Fit number	-	Fit 1	Fit 2	Fit 3	Fit 4
Fitting parameters	4	3	3	5	4
S_0^2	0.98 ± 0.13	0.98	0.98	0.98	0.98
ΔE/ eV	-2 ± 1	0 ± 2	2 ± 2	-1 ± 2	0 ± 1
N_{Ce1}	4	4	2.67	2.67	2.58 ± 0.37
R_{Ce1}/ Å	3.779 ± 0.005	3.771 ± 0.009	3.755 ± 0.009	3.765 ± 0.006	3.768 ± 0.005
σ^2_{Ce1}/ Å^2	0.0059 ± 0.0004	0.0075 ± 0.0003	0.0059	0.0062 ± 0.0002	0.0060 ± 0.0005
N_{Ce2}	-	-	1.33	1.33	-
R_{Ce2}/ Å	-	-	3.838 ± 0.013	4.078 ± 0.051	-
σ^2_{Ce2}/ Å^2	-	-	0.0059	0.0144 ± 0.005	-
R-factor	0.0063	0.0310	0.0301	0.0041	0.0075

Fitting range in k: 4.0–16.8 Å^{-1}; fitting range in R: 3.0–3.9 Å; independent points: 7.22

one of the Ce atoms is significantly shifted from its original position, so its contribution to the regarded EXAFS spectrum becomes very weak. This conclusion is in agreement with the Ce K-edge and Ce L_3-edge XANES data, which indicate that roughly one Ce atom per cornerstone is reduced to Ce^{3+}, which is probably a concomitant effect for the displacement of one Ce atom caused by the reaction with TEMPO and benzyl alcohol. The combined XANES and EXAFS results imply that the originally perfect Ce_6-octahedron is turned into a rigid Ce_5 square pyramid formed by Ce^{4+} ions, while the sixth Ce ion gets reduced to Ce^{3+} and lifted above the equatorial plane with an increased disorder of both static and dynamic origin (Figure 2d).

Such an important distortion of the Ce_6-cluster is not unlikely since previous EXAFS and PDF experiments on the analogous Zr_6 cluster in UiO-66 already showed that the cluster can be reversibly distorted to a comparable extent upon external stimuli.[5,30] A similar distortion was also reported in partially reduced ceria nanoparticles and results from the larger ionic radius of Ce^{3+} (1.03 Å vs. 0.92 Å for Ce^{4+}).[31,32]

A reaction mechanism for the Ce-mediated alcohol oxidation is proposed based on the presence of Ce^{3+} upon exposure to reactants under inert atmosphere (Figure 3). First, one Ce^{4+} in the cluster oxidizes TEMPO to its oxoammonium cation (step a), being reduced itself to Ce^{3+}. The slightly distorted Ce^{3+}-containing cluster is then regenerated by molecular oxygen, thereby closing the Ce cycle. The possible reduction of a second Ce ion in the same cluster is implausible based on the XAS data since only 1/6th of the Ce ions were reduced after 7 h under inert atmosphere, while multiple turnovers were observed for Ce-UiO-66 during the same reaction under oxygen.[13] The oxoammonium cation further reacts with benzyl alcohol to selectively form benzaldehyde while it is reduced to TEMPOH (2,2,6,6-tetramethyl-1-hydroxypiperidine) (step b). The selective oxidation of benzyl alcohol by the oxoammonium cation is often described in literature and the presence of this cation was already reported previously when the reaction was conducted with Ce-UiO-66 under inert atmosphere; a low conversion of benzyl alcohol as well as the detection of TEMPOH pointed towards the oxoammonium cation as an intermediate.[13,33–35] A proton is released during the oxidation of benzyl alcohol and it is hypothesized that it protonates a μ_3-O on the cluster to balance the excess negative charge when one Ce^{4+} is reduced to Ce^{3+}. Charge compensation could also occur through protonation and subsequent detachment of a linker but no evidence for this could be found in the IR spectra (Figure S6). Finally, TEMPOH is swiftly regenerated by molecular oxygen to the initial TEMPO radical (step c), thereby closing the TEMPO cycle. Steps (b) and (c) are known to be much faster than step (a) since numerous catalyst systems involving these two reactions have been described with a much higher rate than reported for Ce-UiO-66.[26,36,37] Therefore, the overall activity could be increased by improving the oxoammonium formation rate (step a).

The reaction rate of the TEMPO oxidation strongly depends on the accessibility of Ce in the cluster. The pore aperture of Ce^{4+}-MOFs should therefore be sufficiently large to allow diffusion of TEMPO through their pore network. In addition, there should be open coordination sites available on the cluster to interact with incoming reactants, which directly implies that the (average) number of linkers surrounding each cluster should be lower than the maximum twelve. A clear illustration of the effect of node connectivity on catalytic performance of analogous Zr-MOFs can be found in the work of Farha et al.[38] Besides UiO-66, which contains 12-connected clusters (in the absence of defects), NU-1000 and MOF-808, bearing, respectively eight-fold and six-fold coordinated clusters, were compared for their catalytic activity in the hydrolysis of dimethyl 4-nitrophenyl phosphate, a nerve-agent simulant. The reported turnover frequencies of 0.004 s^{-1}, 0.09 s^{-1} and >1.4 s^{-1} respectively for UiO-66, NU-1000 and MOF-808, clearly indicate the benefit of low-coordinated clusters on catalytic activity.[38]

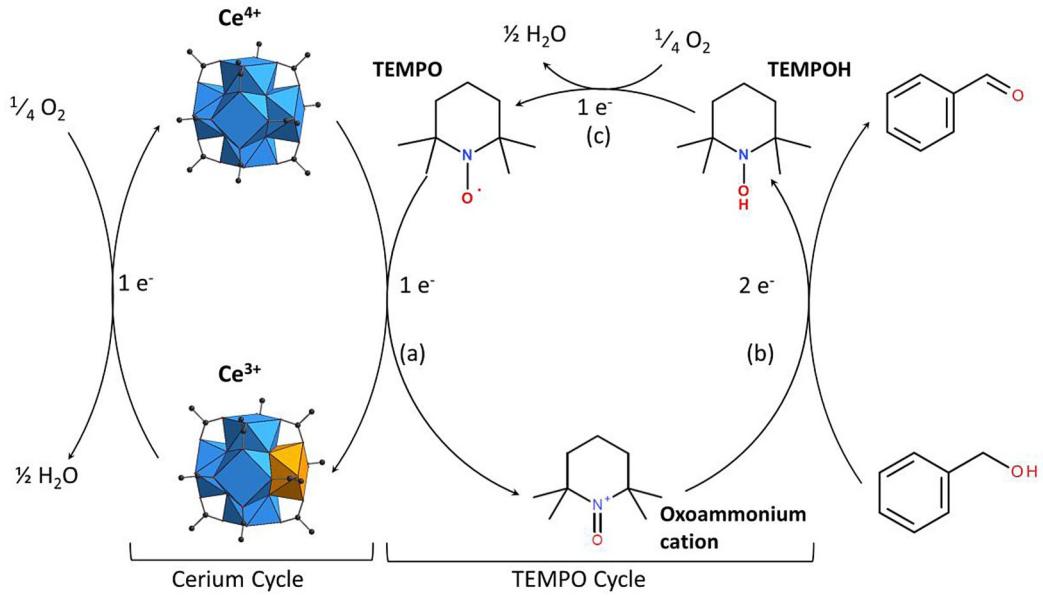

Figure 3. Proposed reaction mechanism for the aerobic TEMPO-mediated oxidation of benzyl alcohol by Ce^{4+}-MOFs.

While previous work demonstrated the activity of Ce-UiO-66 and Ce-UiO-66-ndc (ndc = 2,6-naphthalenedicarboxylate) in aerobic alcohol oxidations, the reaction rate was limited by pore size and the number of open sites originating from missing linker defects.[13] Here, we report an improved catalytic activity for the TEMPO-mediated aerobic oxidation of benzyl alcohol by replacing Ce-UiO-66 with Ce-MOF-808 ($[Ce_6O_4(OH)_4(btc)_2(OH)_6]$; btc = trimesate), a large-pore MOF with the lowest connectivity of all known MOFs based on the same M_6-clusters (M = Zr, Hf, Ce).[21,22,39,40]

The activity of Ce-MOF-808 was tested under reaction conditions identical to those of the oxidation of benzyl alcohol by Ce-UiO-66.[13] The activation procedure of Ce-MOF-808 was adapted to its lower thermal stability, that is, the activation temperature was decreased to 100 °C and vacuum was applied to ensure complete evacuation of the pores.[22] The resulting Ce-MOF-808 outperformed all previously tested Ce^{4+}-MOFs (Table 2). After seven hours, Ce-MOF-808 converted 97% of the benzyl alcohol, which is much higher than the previously reported Ce-UiO-66 (29%) and Ce-UiO-66-ndc (80%).[13] The improved activity is due to the large pore size and low connectivity of Ce-MOF-808: the clusters are 6-fold connected by trimesate linkers. Liquid ^{1}H NMR of a digested sample revealed the presence of 2 additional coordinating formates leading to four remaining open sites that can act as active sites during reaction (Figure S2). The structural integrity of Ce-MOF-808 during activation and reaction was demonstrated via PXRD (Figure S5) and the heterogeneity of the catalyst was proven by a hot filtration test: after 2 h reaction; Ce-MOF-808 was removed and no further reaction was observed (Figure S7).

Table 2. Comparison of benzyl alcohol conversion using various Ce^{4+}-MOFs.

Catalyst	Activation temperature [°C]	Conversion [%]
Ce-UiO-66[13]	180	29
Ce-UiO-66-NDC[13]	180	80
Ce-MOF-808	100	97
6 bar O_2, 110 °C, 7 h, CH_3CN, 10 mol% Ce, 30 mol% TEMPO		

In conclusion, the redox behavior of Ce^{4+}-MOFs was investigated using a combined XANES and EXAFS approach, focusing on the Ce oxidation state and the geometry of the active site. One Ce ion could be reduced per cluster, thereby moving slightly away from the center of the cluster. This unambiguously demonstrates the redox activity of Ce-MOFs, paving the way for their further application in redox catalysis. This was exemplified by the development of a catalytic system with Ce-MOF-808 which displayed an increased activity for the aerobic TEMPO-mediated oxidation of benzyl alcohol.

Acknowledgements

S.S., B.B., and D.D.V. gratefully acknowledge the FWO Flanders for funding (Aspirant grant and postdoctoral grant). CL and ALB acknowledge the Mega-Grant of the Russian Federation Government (14.Y26.31.0001). The XAS experiments were performed on beamline BM31 at the European Synchrotron Radiation Facility (ESRF), Grenoble, France. We are grateful to Michela Brunelli and Hermann Emerich at the ESRF for providing assistance in using beamline BM31.

Conflict of interest

The authors declare no conflict of interest.

Keywords: catalysis · cerium · metal–organic frameworks · redox chemistry · X-ray spectroscopy

[1] J. Liu, L. Chen, H. Cui, J. Zhang, L. Zhang, C.-Y. Su, *Chem. Soc. Rev.* **2014**, *43*, 6011 – 6061.
[2] H. Kim, S. Yang, S. R. Rao, S. Narayanan, E. A. Kapustin, H. Furukawa, A. S. Umans, O. M. Yaghi, E. N. Wang, *Science* **2017**, *356*, 430 – 434.
[3] J. R. Li, J. Sculley, H. C. Zhou, *Chem. Rev.* **2012**, *112*, 869 – 932.
[4] J. H. Cavka, S. Jakobsen, U. Olsbye, N. Guillou, C. Lamberti, S. Bordiga, K. P. Lillerud, *J. Am. Chem. Soc.* **2008**, *130*, 13850 – 13851.
[5] L. Valenzano, B. Civalleri, S. Chavan, S. Bordiga, M. H. Nilsen, S. Jakobsen, K. P. Lillerud, C. Lamberti, *Chem. Mater.* **2011**, *23*, 1700 – 1718.
[6] S. Jakobsen, D. Gianolio, D. S. Wragg, M. H. Nilsen, H. Emerich, S. Bordiga, C. Lamberti, U. Olsbye, M. Tilset, K. P. Lillerud, *Phys. Rev. B* **2012**, *86*, 125429.
[7] T. Montini, M. Melchionna, M. Monai, P. Fornasiero, *Chem. Rev.* **2016**, *116*, 5987 – 6041.
[8] F. Vermoortele, R. Ameloot, A. Vimont, C. Serre, D. De Vos, *Chem. Commun.* **2011**, *47*, 1521 – 1523.
[9] F. Vermoortele, B. Bueken, G. Le Bars, B. Van de Voorde, M. Vandichel, K. Houthoofd, A. Vimont, M. Daturi, M. Waroquier, V. Van Speybroeck, C. Kirschhock, D. De Vos, *J. Am. Chem. Soc.* **2013**, *135*, 11465 – 11468.
[10] F. Vermoortele, M. Vandichel, B. Van De Voorde, R. Ameloot, M. Waroquier, V. Van Speybroeck, D. E. De Vos, *Angew. Chem. Int. Ed.* **2012**, *51*, 4887 – 4890; *Angew. Chem.* **2012**, *124*, 4971 – 4974.
[11] C. Caratelli, J. Hajek, F. G. Cirujano, M. Waroquier, F. X. Llabrés i Xamena, V. Van Speybroeck, *J. Catal.* **2017**, *352*, 401 – 414.
[12] G. W. Peterson, S. Y. Moon, G. W. Wagner, M. G. Hall, J. B. Decoste, J. T. Hupp, O. K. Farha, *Inorg. Chem.* **2015**, *54*, 9684 – 9686.
[13] M. Lammert, M. T. Wharmby, S. Smolders, B. Bueken, A. Lieb, K. A. Lomachenko, D. De Vos, N. Stock, *Chem. Commun.* **2015**, *51*, 12578 – 12581.
[14] V. Nair, A. Deepthi, *Chem. Rev.* **2007**, *107*, 1862 – 1891.
[15] V. Sridharan, J. C. Menéndez, *Synthesis* **2010**, *110*, 3805 – 3849.
[16] A. Trovarelli, C. de Leitenburg, M. Boaro, G. Dolcetti, *Catal. Today* **1999**, *50*, 353 – 367.
[17] Z. Wu, R. Jin, Y. Liu, H. Wang, *Catal. Commun.* **2008**, *9*, 2217 – 2220.
[18] S. Carrettin, P. Concepción, A. Corma, J. M. López Nieto, V. F. Puntes, *Angew. Chem. Int. Ed.* **2004**, *43*, 2538 – 2540; *Angew. Chem.* **2004**, *116*, 2592 – 2594.
[19] R. Si, M. Flytzani-Stephanopoulos, *Angew. Chem. Int. Ed.* **2008**, *120*, 2926 – 2929; *Angew. Chem.* **2008**, *120*, 2968 – 2970.
[20] R. Wang, P. A. Crozier, R. Sharma, J. B. Adams, *nanoletters* **2008**, *8*, 962 – 967.
[21] M. Lammert, H. Reinsch, C. A. Murray, M. T. Wharmby, H. Terraschke, N. Stock, *Dalton Trans.* **2016**, *45*, 18822 – 18826.
[22] M. Lammert, C. Glißmann, H. Reinsch, N. Stock, *Cryst. Growth Des.* **2017**, *17*, 1125 – 1131.
[23] M. Lammert, C. Glißmann, N. Stock, *Dalton Trans.* **2017**, *46*, 2425 – 2429.
[24] A. C. Dreischarf, M. Lammert, N. Stock, H. Reinsch, *Inorg. Chem.* **2017**, *56*, 2270 – 2277.
[25] S. L. Estes, M. R. Antonio, L. Soderholm, *J. Phys. Chem. C* **2016**, *120*, 5810 – 5818.
[26] S. S. Kim, H. C. Jung, *Synthesis* **2003**, *14*, 2135 – 2137.
[27] S. Bordiga, E. Groppo, G. Agostini, J. A. Van Bokhoven, C. Lamberti, *Chem. Rev.* **2013**, *113*, 1736 – 1850.

[28] J. J. Rehr, C. H. Booth, F. Bridges, S. I. Zabinsky, *Phys. Rev. B* **1994**, *49*, 12347 – 12350.
[29] D. E. Ramaker, D. C. Koningsberger, *Phys. Chem. Chem. Phys.* **2010**, *12*, 5514 – 5534.
[30] A. E. Platero-Prats, A. Mavrandonakis, L. C. Gallington, Y. Liu, J. T. Hupp, O. K. Farha, C. J. Cramer, K. W. Chapman, *J. Am. Chem. Soc.* **2016**, *138*, 4178 – 4185.
[31] S. Deshpande, S. Patil, S. V. Kuchibhatla, S. Seal, *Appl. Phys. Lett.* **2005**, *87*, 133133.
[32] M. Nolan, S. C. Parker, G. W. Watson, *Surf. Sci.* **2005**, *595*, 223 – 232.
[33] A. Dijksman, I. W. C. E. Arends, R. A. Sheldon, *Chem. Commun.* **1999**, *2*, 1591 – 1592.
[34] R. A. Sheldon, I. W. C. E. Arends, G. J. Ten Brink, A. Dijksman, *Acc. Chem. Res.* **2002**, *35*, 774 – 781.
[35] A. Badalyan, S. S. Stahl, *Nature* **2016**, *535*, 406 – 410.
[36] A. Dijksman, I. W. C. E. Arends, R. A. Sheldon, *Org. Biomol. Chem.* **2003**, *1*, 3232.
[37] M. F. Semmelhack, C. R. Schmid, D. A. Cortés, *Tetrahedron Lett.* **1986**, *27*, 1119 – 1122.
[38] S. Y. Moon, Y. Liu, J. T. Hupp, O. K. Farha, *Angew. Chem. Int. Ed.* **2015**, *66*, 6795 – 6799.
[39] Y. Bai, Y. Dou, L.-H. Xie, W. Rutledge, J.-R. Li, H.-C. Zhou, *Chem. Soc. Rev.* **2016**, *45*, 2327 – 2367.
[40] M. J. Cliffe, W. Wan, X. Zou, P. A. Chater, A. K. Kleppe, M. G. Tucker, H. Wilhelm, N. P. Funnell, F.-X. Coudert, A. L. Goodwin, *Nat. Commun.* **2014**, *5*, 4176.

Manuscript received: August 31, 2017
Accepted manuscript online: October 13, 2017
Version of record online: November 15, 2017